Supplemental Information

for

Reducing Secondary Organic Aerosol Formation from Gasoline Vehicle Exhaust

Yunliang Zhao[a,b], Rawad Saleh[a,b,1], Georges Saliba[a,b], Albert A. Presto[a,b], Timothy D. Gordon[a,2], Greg T. Drozd[c], Allen H. Goldstein[c], Neil M. Donahue[a,d], Allen L. Robinson[a,b,3]

[a]Center for Atmospheric Particle Studies, Carnegie Mellon University, Pittsburgh, PA, USA, 15213;
[b]Department of Mechanical Engineering, Carnegie Mellon University, Pittsburgh PA, USA, 15213;
[c]Department of Environmental Science, Policy and Management, University of California, Berkeley, CA, USA, 94720;
[d]Department of Chemical Engineering, Carnegie Mellon University, Pittsburgh, PA, USA, 15213
[1]Now at: College of Engineering, University of Georgia, Athens, GA, USA, 30602;
[2]Now at: Handix Scientific, Boulder, CO, USA, 80301
[3]To whom correspondence should be addressed. Email: alr@andrew.cmu.edu

This supplemental information includes:
Methods used to characterize the primary emissions, determine the SOA production and predict SOA production of measured SOA precursors.
Figure S1-S9
Table S1-S9

Materials and Methods

Characterization of tailpipe emissions from on-road gasoline vehicles and their SOA production was carried out during dynamometer testing at the California Air Resources Board's (CARB) Haagen-Smit Laboratory. The test fleet consisted of 59 on-road gasoline vehicles, spanning a wide range of model years and emission control technologies/standards. All of these vehicles were tested for primary emissions. A subset of these vehicles (*n*=25) was tested for SOA formation in a smog chamber. Table S1 compiles the information of the test fleet, primary emissions measurements and photo-oxidation experiments. The detailed description of the experimental setup and procedure has been provided elsewhere (1, 2). Only a brief discussion is provided here.

Test Fleet, Fuel and Test Cycle. For discussion, the 59 tested vehicles were categorized into four groups based on emission certification standards as 14 pre-LEV vehicles (Tier0 and Tier1), 18 LEV vehicles (transitional low emission vehicles and low emission vehicles) and 19 ULEV vehicles (Ultra-low emission vehicles) and 8 SULEV vehicles (Super ultra-low and partial zero emission vehicles). The SULEV category includes both port and direct injection vehicles (Table S1). There are 6 vehicles whose specific emission standards were unknown. We have classified them as LEV vehicles if there were certificated as LEV I vehicles (*n*=*3*) and classified them as ULEV vehicles if these vehicles were certificated as LEV II vehicles (*n*=*3*). Our categorization reflects reductions in emissions due to the tightening of emissions standards (Fig. S6).

All vehicles were tested on a cold-start Unified Cycle (UC) using the same California commercial summer gasoline fuel. The UC is designed to simulate driving in the Sothern California. The UC consists of three bags, similar to the Federal Test Procedure (FTP)-75, but is a more aggressive cycle with higher speeds, higher acceleration, fewer stops and less idling time. Two of these vehicles were also tested on a hot-start UC.

Measurements of Primary Emissions. The entire exhaust from a gasoline vehicle during each test was diluted in a constant volume sampler (CVS) using clean air treated by high efficient particulate filters. Comprehensive characterization of primary emissions was carried out by directly sampling the dilute exhaust from the CVS using an AVL-AMA 4000 system. Gas-phase organics were measured by flame ionization detection (FID), methane by gas chromatography (GC)-FID, NO_x by chemiluminescence, and CO and CO_2 by nondispersive infrared detection. The gas-phase organics include both hydrocarbons and oxygenated compounds. Therefore, for discussion, we define the organics measured by FID as organic gases. Non-methane organic gases (NMOG) were defined as the difference between total organic gases and methane. However, one should note that the amount of oxygenated compounds measured by FID was underestimated (3) because the FID was calibrated with a methane/propane blend.

Comprehensive speciation analysis of NMOG was performed for most tests (Table S1). The dilute exhaust was sampled from the CVS into Tedlar® bags and analyzed by GC following the CARB test methods MLD 102 and 103(4) to quantify more 200 hydrocarbon species (Dataset S1) that spanned the carbon number range of 2 to 12, including straight alkanes (*n*-alkanes), branched alkanes (*b*-alkanes), alkenes, cycloalkanes, single-ring aromatic compounds. Oxygenated compounds, including alcohols, aldehydes and ketones, were quantified using the CARB test methods MLD 101 and 104 (5, 6). IVOCs and SVOCs were quantified following the approach of Zhao et al.(7, 8)

IVOCs and SVOCs were characterized for a subset of vehicles (8) (Table S1). In brief, IVOCs and SVOCs were collected by sampling the dilute exhaust from the CVS through a quartz filter immediately followed by two adsorbent tubes (Gerstel 6 mm OD, 4.5 mm ID glass tube filled with ~290 mg of Tenax® TA), all connected in series. This sampling train was housed inside a temperature-controlled box, maintained at ~47°C mimicking the CFR86 protocol. Both adsorbent tubes and the quartz filters were analyzed by gas chromatography-mass spectrometry (GC/MS) (Agilent, 6890 GC/5975 MS) equipped with a Gerstel thermal desorption and injection system (Gerstel, Baltimore, MD) and a capillary column (Agilent HP-5MS, 30 m × 0.25 mm). The peak thermal desorption temperature was 275 °C for adsorbent tubes and 300 °C for quartz filters. The detailed description of quantification of IVOCs can be found elsewhere(7, 8).

In this study, IVOCs were defined as compounds in the retention-time range of C_{12}~C_{22} *n*-alkanes desorbed from adsorbent tubes. The total IVOCs in each sample were quantified by binning the total ion chromatogram acquired during GC/MS analysis of the adsorbent tube into 11 bins based on the retention time of C_{12}~C_{22} *n*-alkanes. Each bin was centered at one *n*-alkane and defined the "B_n" bin where "*n*" was the carbon number of the *n*-alkane in that bin. The amount of IVOCs in each bin was determined by the total ion signal in that bin divided by the response factor of the *n*-alkane in that bin.

Speciation analysis of IVOCs was also performed. 57 individual species, including *n*-alkanes, *b*-alkanes, cyclic alkanes and aromatics, were quantified. In sum, these compounds only accounted for 16±6% of total IVOCs(8). The unspeciated IVOCs, defined as the difference between total IVOCs and speciated IVOCs, were composed of a complex mixture of co-eluted compounds, which cannot be resolved on a molecular basis through the traditional GC/MS analysis. This material is often referred to as an unresolved complex mixture (UCM). These unspeciated IVOCs were classified into unspeciated *b*-alkanes and unspeciated cyclic compounds in each retention-time based bin based on their mass spectra (7, 8). We present the emission factors of speciated IVOCs, unspeciated *b*-alkanes and cyclic compounds in each of 11 bins in Dataset S2.

SVOCs were defined as the organics collected on quartz filters and two adsorbent tubes in the retention time range of C_{23}~C_{32} *n*-alkanes. SVOCs

desorbed from the quartz filters were quantified using the same approach as the one for IVOCs.

A different approach was used for quantification of SVOCs desorbed from adsorbent tubes. SVOCs desorbed from adsorbent tubes were quantified using *m/z 57*, instead of the total ion signal, because of substantial interference of products from the reactions of NO_x and adsorbent Tenax TA (9) on the total ion signal in the SVOC retention-time range and difficulty to separate the interference from signals produced by organics in tailpipe emissions. However, interference of these products on the signal of *m/z 57* was negligible. In addition, the signal of *m/z 57* was detected across the retention time range of SVOCs.

SVOCs desorbed from adsorbent tubes were quantified by binning the chromatogram of *m/z 57* into 10 bins based on the retention time of C_{23}~C_{32} *n*-alkanes with each bin centered at one *n*-alkane. The mass of *m/z 57* in each bin was calculated using the response factor of *m/z 57* determined by the *n*-alkane. The mass of *m/z 57* in each bin was converted to total organics by assuming the fraction of *m/z 57* in that bin to be same as the average fraction of *m/z 57* in the same bin of SVOCs desorbed from quartz filters.

We did not characterize the chemical composition of SVOCs in this study. However, SVOCs are likely dominated by cyclic alkanes(10). The emission factors of SVOCs are compiled in Dataset S3.

The emissions of speciated VOCs, IVOCs and SVOCs were not measured for all of tests (Table S1). However, speciated VOCs and IVOCs are strongly correlated with NMOG. For example, the linear regression yields the slope of 0.2 and R^2=0.93 for single-ring aromatic compounds versus NMOG and 0.04 and R^2=0.92 for IVOCs versus NMOG. Therefore, for experiments where IVOCs and speciated VOC were not measured, these emissions were estimated based on bulk NMOG emission factor and the chemical composition of speciated VOCs and IVOCs from the average test.

SVOCs are a major component of POA and likely attributed to the lubricant oil(10), differing from single-ring aromatics and IVOCs originating from gasoline fuel. Measured SVOC emissions follow a similar trend to POA emissions (Fig. S6D, Fig. S8), but a strong correlation was not found between SVOC and POA emissions. The SVOCs for the tests without SVOC measurements were estimated based on the median ratio between measured SVOCs and POA in each class of vehicles (0.85 for pre-LEV, 1.25 for LEV, 1.19 for ULEV). POA was the organics collected by a bare quartz filter. For SULEV vehicles, the median SVOC-to-POA ratio for ULEV vehicles was used as ULEV and SULEV vehicles were new and met the same PM emission standard(11).

Photo-oxidation Experiments. Photo-oxidation experiments were conducted for 25 vehicles, a subset of total tested vehicles, including 4 pre-LEV, 6 LEV, 8

ULEV and 7 SULEV vehicles (Table S1). The key parameters and results of photo-oxidation experiments are summarized in Table S2.

The photo-oxidation experiments were conducted using the Carnegie Mellon's mobile environmental chamber. This mobile chamber is a 7 m^3 Teflon® bag suspended in a metal frame (12) and was located indoors during this study. We conducted a total of 33 photo-oxidation experiments (5 pre-LEV, 7 LEV, 12 ULEV and 9 SULEV experiments) (Table S2). The number of photo-oxidation experiments was greater than the number unique vehicles because some of the vehicles were tested more than once. Before each experiment, the chamber was flushed overnight using clean air treated by silica gel, HEPA filters and activated charcoal in series and with the chamber UV lights (Model F40BL UVA, General Electric) turned on.

The dilute exhaust was drawn from the CVS and injected into the chamber by a Dekati® diluter through silcosteel® stainless steel tubing. Both the diluter and transfer line were electrically heated and maintained at ~47°C, matching the filter and Tenax collection temperature. For eleven of these experiments we only filled the chamber during the period of the first UC bag. For the rest of these experiments we filled the chamber through the entire UC, except for the 10-min hot-soak period. The NMOG emissions are dominated by the period of the first UC bag, especially for newer vehicles. The concentration of NMOG in the

chamber was approximately the same between the first UC bag and the entire UC, especially for experiments for SULEV vehicles.

Following the injection of dilute exhaust, we injected ammonium-sulfate seed particles into the chamber using a constant-output atomizer (TSI, model 3075) followed by a diffusion dryer and a neutralizer. These seed particles increased the condensational sink to reduce loss of condensable vapors to the chamber walls; we also used them to determine the particle wall losses during each experiment.

Nitrous acid (HONO) was added to the chamber as a hydroxyl radical (OH) source. We added HONO into the chamber by bubbling clean air through a solution prepared by mixing 0.1 M $NaNO_2$ and 0.05 M H_2SO_4 with a volume ratio of 1:2. A known amount of butanol-d_9 (Cambridge Isotope Laboratories, MA) was added to determine the OH concentration. Propene was also added to adjust the NMOG to NO_x ratio (NMOG:NO_x) nominally to a typical urban level of ~3:1 ppb C/ppb NO_x (1). However, the interference of HONO on chemiluminescence NO_x measurements (13) led to addition of excess propene in the beginning of experiments. As a result, the initial NMOG:NO_x varied substantially by vehicle class, although in all cases the NMOG:NOx would have been around 3 following the complete photolysis of HONO. In this work the amount of NMOG used to calculate the initial NMOG:NO_x was the sum of NMOG in the exhaust, propene, and d_9-butanol added to the chamber. The amount of NO_x used to calculate the

initial NMOG:NO_x was the NO measured by the NO_x monitor. Consequently, the NMOG:NO_x we employed in our analysis and calculations are empirical and should be applied in other applications with caution; however, the strong empirical correlations support our conclusion. After all gases and particles were injected and became well-mixed, the UV lights were switched on to initiate the photo-oxidation reactions.

The temporal evolution of particles and gases in the chamber was characterized by a suite of instruments. The particle number and volume in the chamber were measured using a scanning mobility particle sizer (SMPS, TSI classifier model 3080, CPC model 3772 or 3776). The nonrefractory submicron particle mass and chemical composition were measured by a high-resolution time-of-flight aerosol mass spectrometer (HR-tof-AMS, Aerodyne, Inc., MA). CO_2 was measured by a LI-820 monitor (Li-COR Biosciences, NE); NO_x, CO and O_3 was measured by API-Teledyne T200, T300 and 400A analyzers, respectively. The concentration of butanol-d_9 was measured by proton transfer reaction-mass spectrometry (Ionicon, Austria).

The NMOG concentration in the chamber associated with the exhaust was not measured. Instead, the initial NMOG concentration in the chamber was calculated based on the NMOG concentration measured in the CVS and the dilution ratio determined by CO_2 measured in the CVS and the chamber concurrently. The dilution ratio determined by CO_2 was confirmed by

independent measurements of CO and NO_x. The decay of total NMOG was unknown, but reacted speciated VOCs, IVOCs and SVOCs can be predicted based on their initial concentration and OH exposure derived from the decay of butanol-d_9 or aromatics when butanol-d_9 was not added.

Both particle and organic vapor wall losses were estimated in order to determine the SOA production. In the present study, the organic vapors were assumed to maintain equilibrium with both suspended and wall-bound particles (1, 14). Therefore, the SOA production (C_{SOA}, $\mu g/m^3$) over a period of photo-oxidation was calculated by:

$$C_{SOA}(t) = \left(\frac{C_{OA,sus}(t)}{C_{seed,sus}(t)} - \frac{C_{OA,sus}(t=0)}{C_{seed,sus}(t=0)}\right) \times C_{seed,sus}(t=0)$$

Where $C_{OA,sus}(t)$ and $C_{seed,sus}(t)$ are the concentrations of suspended OA and seed particles (ammonium sulfate); t=0 refers to the time when the UV lights were switched on. The $C_{OA,sus}(t)$-to-$C_{seed,sus}(t)$ ratio was directly measured by HR-tof-AMS. The contribution of POA to suspended OA was determined by the $C_{OA,sus}(t=0)$-to-$C_{seed,sus}(t=0)$ ratio multiplied by $C_{seed,sus}(t=0)$. The concentration of $C_{seed,sus}(t=0)$ was calculated based on the particle volume measured by SMPS and the $C_{OA,sus}(t=0)$-to-$C_{seed,sus}(t=0)$ ratio measured by HR-tof-AMS. An inorganic density of 1.77 g/cm^3 (14) and an organic density of 1.0 g/cm^3 (15) were used to distinguish ammonium sulfate from primary OA and convert the volume to the mass.

Dynamic Blank of SOA. In addition to experiments with dilute exhaust, photo-oxidation experiments were also conducted when the CVS was operated on clean air (no exhaust) for the same period as a standard UC. The addition of HONO, ammonium sulfate seed particles, d_9-butanol and propene followed the same procedure described above. Gases and particles were characterized using the same array of instruments. The SOA formation during these experiments was defined as dynamic blanks. The dynamic blanks were converted to emission factors using the average carbon emission across all tests. The dynamic blanks likely overestimate the SOA production from background organics because operating CVS on clean air promotes evaporation of organics condensed on the CVS walls.

Vapor Wall Loss and Condensational Sink. The wall losses of condensable vapors during the smog-chamber experiments could lead to the underestimation of SOA production, which, in turn, could underestimate the effective SOA yield(16). Although it is difficult to quantify the vapor wall losses, it depends on the condensational sink(16). To examine whether higher effective SOA yields for LEV and ULEV vehicles than pre-LEV vehicles were caused by lower organic vapor wall losses, we have calculated the condensational sink caused by suspended particles for organic vapors following the approach of Saleh et al.(17) and Trump et al.(18). A smaller condensational sink of suspended particles indicates a larger fraction of organic vapors losing to the walls compared to their condensation onto suspended particles(17).

To be conservative, we calculated the condensational sink of suspended particles at the end of photo-oxidation experiments, when the particle number concentration was lowest due to wall losses. The measured particle size distribution was used in the calculation. We assumed a mass accommodation coefficient of unity and an average molecular weight of organic vapors of 200 g/mol.

The average condensational sink in experiments for pre-LEV vehicles (0.44±0.33 min^{-1}) was comparable to the averages for LEV (0.57±0.33 min^{-1}), ULEV vehicles (0.39±0.19 min^{-1}) and SULEV vehicles (0.37±0.23 min^{-1}). This means that the vapor wall loss rates should be similar across the different classes of vehicles. Therefore, the similarity in the condensational sink means that the higher effective SOA yields for LEV and ULEV vehicles than Pre-LEV vehicles were **not** due to the biases caused by organic vapor wall losses.

In this study, we estimated the wall losses of condensable vapors by assuming that condensable vapors maintain equilibrium with both suspended and wall-bound particles (Method#1) to calculate SOA production. To evaluate performance of this method#1 in accounting for the vapor wall losses, we also estimated the condensable vapor losses to chamber walls by assigning a condensational sink to the chamber walls. The condensational sink of the chamber walls was assumed to be in the range of 0.1 to 0.14 min^{-1}(19)

(Method#2), which was determined using an 8 m^3 smog chamber, similar to the size of our chamber. We assumed the accommodation coefficients of 0.1 and 1 for suspended particles.

Fig. S9 compares SOA production after correcting for vapor wall losses calculated through the method#1 and #2 in a photo-oxidation experiment for a ULEV vehicle. Saleh et al.(17) has reported a mass accommodation coefficient of order 0.1 for the SOA produced during alpha-pinene ozonolysis. The comparisons in Fig. S9 show that our approach of determining SOA production (method#1) accounts for vapor wall losses if the published condensational sink of the chamber walls(19) is applicable to our chamber.

The OH concentration and reaction rate also influences the vapor wall losses. Lower OH concentrations (slower reaction rates) results in higher vapor wall losses. The median OH exposure estimated in our study was 6.8×10^6, 8.1×10^6, 1.1×10^7 molecules cm^{-3} h for experiments with pre-LEV, LEV and ULEV vehicles, respectively. Therefore there are only modest differences (less than a factor of 2) in OH concentration across the experiments. Although the pre-LEV experiments have lower OH concentrations, they have larger condensational sink of suspended particles compared to ULEV experiments. The large condensational sink reduces the vapor wall losses. The effective SOA yield was determined using the measured SOA production divided by reacted SOA precursors. Even if we assume that all IVOCs and SVOCs are lost to walls in pre-LEV experiments,

which is unlikely, the increase in the effective SOA yield for pre-LEV experiments is less than a factor of 1.5 because the sum of reacted IVOCs and SVOCs contribute only 30%, on average, of total reacted SOA precursors. Therefore, the amount of vapor losses to the walls due to OH exposure has little influence on the trend of the observed effective SOA yields across the different vehicle classes.

Calculating SOA Production from VOCs, IVOCs and SVOCs

SOA production (ΔM) from an individual SOA precursor (HC_i) over a period (Δt) was calculated using:

$$\Delta M = [HC_i] \times (1 - e^{-k_{OH,i} \times [OH] \times \Delta t}) \times Y_i$$

Where [HC_i] is the initial concentration of the compound *i* in the chamber (μg m^{-3}); $k_{OH,i}$ is its OH reaction rate constant (25°C, molecules cm^{-3}); [OH] is the concentration of hydroxyl radicals; Y_i is the SOA yield of the compound *i*. The total SOA production is the sum of the SOA production from all precursors. To estimate SOA production during each photo-oxidation experiment, the OH exposure ([OH]×Δt) was calculated based on the measured decay of butanol-d_9 or single-ring aromatics for experiments with no addition of butanol-d_9. The SOA yield for each compound is taken from published parameterizations derived from chamber experiments and the wall-loss corrected OA concentration at the end of each experiment in this study. For compounds with no published SOA yield data, we assigned surrogate compounds. The OH reaction rate constants and SOA yield parameters are listed in Tables S3-S9. A detailed discussion of assigning

surrogates can be found elsewhere(7, 8, 20). A brief description is provided below.

SOA Production from VOCs. The speciated VOCs were lumped into the SAPRC-07 mechanisms (21). Speciated VOCs considered to be SOA precursors included benzene, ARO1, ARO2 and ALK5. The SOA yields for these lumped species were taken from published CMAQ parameters in Carlton et al. (22) accounting for the wall-loss corrected OA concentration measured at the end of each experiment. Some of the speciated VOCs in ARO1 and ARO2 were likely quantified as IVOCs. Therefore, these speciated VOCs were removed from ARO1 and ARO2 to avoid double counting of the SOA precursors based on their retention time indices, although they accounted for less than 1%, on average, of species in ARO1 and ARO2.

Although the reaction of unsaturated organics with ozone and NO_3 radicals can form SOA (23, 24), alkenes are not significant source of SOA in gasoline-vehicle exhaust. The alkenes in vehicle exhaust are dominated by small molecules, with C_2-C_4 alkenes accounting for 88%±11% of total measured alkenes. Keywood et al.(23) showed that SOA yields from alkene ozonolysis are low. For example, the SOA yield of cylcopentene is less than 1% at the typical OA concentration of chamber experiments in our study. The SOA yields of C_2-C_4 alkenes that dominate vehicle exhaust are even lower than cyclopentene, suggesting negligible contribution to SOA. This conclusion is supported by the lack of

correlation between the ozone concentration and effective SOA yield (Fig. S3). For alkenes-NO_3 reactions, Gong et al., (24) reported that the SOA formation was only observed for ≥C_7 linear alkenes. We measured no emissions of these larger alkenes (concentrations were below method detection limits in our experiments).

Propene and butanol-d_9 were added in the beginning of experiments. Both published laboratory data (23-25) and the blank experiments in this study demonstrate that these compounds do not contribute measurable SOA. This is also demonstrated by SULEV experiments, which had similar OH exposure and ozone concentration compared to the LEV and ULEV experiments but exhibited low SOA production similar to dynamic blanks.

SOA production from IVOCs. The SOA production from IVOCs was calculated using the approach of Zhao et al. (7, 8). For speciated IVOCs, the OH rate constants are either taken from the literature (26) or calculated based on the structure-reactivity relationship (27). SOA yields for each speciated IVOC are based on published results from photo-oxidation experiments (20, 28-31) accounting for wall loss corrected OA concentration measured at the end of each experiment. For unspeciated IVOCs, surrogate compounds are assigned to unspeciated *b*-alkanes and unspeciated cyclic compounds in each of 11 retention-time based bins to represent their OH rate constants and SOA yields.

The selection of surrogate compounds accounted for the effects of molecular structure and volatility on OH reaction rate constants and SOA yields (7, 8).

Both aromatic compounds and cyclic alkanes are likely major contributors to unspeciated cyclic IVOC compounds(8). Therefore, both surrogate compounds of n-alkanes and naphthalenes were used to bound SOA production from unspeciated cyclic compounds. SOA production from unspeciated cyclic IVOC compounds in this present study is considered as the average of SOA production estimated using *n*-alkanes and naphthalenes as surrogate compounds(8).

SOA production from SVOCs. SVOCs are organics that elute between C_{23}~C_{32} *n*-alkanes during the GC/MS analysis (32) and are likely dominated by cyclic alkanes (10). In this study, SVOCs are considered as one lumped component with an SOA yield and OH reaction rate constant represented by the C_{23} *n*-alkane.

Estimating SOA yields under high- and low-NO_x conditions. The SOA yields for VOCs (benzene, ARO1, ARO2 and ALK5) under high-NO_x conditions are from Carlton et al. (21). The SOA yields for IVOCs and SVOCs under high-NO_x conditions are from Chan et al. (20), Lim and Ziemann (29), Presto et al. (30) and Hunter et al.(28).

The SOA yields for single-ring aromatic compounds and naphthalenes under low-NO_x conditions do not depend on the OA concentration (20, 33) and they are from Ng et al.(33) and Chan et al.(20).

There is limited data on the SOA yield for alkanes under low-NO_x conditions. Cappa et al. (31) and Loza et al. (34) reported SOA yields for four C_{12} alkanes (dodecane, *2*-methyleundecane, *n*-hexylcyclohexane and cyclododecane) under low-NO_x conditions. No other data are available to derive the SOA yields under low-NO_x conditions for alkanes with larger carbon number, which are a major contributor to both IVOCs (8) and SVOCs(10). For the four studied alkanes, the SOA yields at the OA concentration of 10 μg/m^3 are similar under high- and low-NO_x conditions, except for cyclododecane (31). Therefore, we assume that SOA yields for alkanes do not depend on NO_x (they are the same for low and high NOx conditions). Cyclic alkanes in IVOC and SVOC range likely dominated by cyclic alkanes with one or more rings and one or more branched alkyl side chains (10, 35). Alk5 is dominated by *n*- and *b*-alkanes (Fig. 2A).

Effective SOA Yield. The effective SOA yield in each experiment is calculated using the measured SOA mass divided by the mass of reacted SOA precursors at the end of each experiment. The following compounds are considered to be SOA precursors: selected VOCs (benzene, ARO1, ARO2 and ALK5), all IVOCs and all SVOCs. The analysis accounts for the different OH rate constants for

each precursor (Tables S5 and S9). The OH rate constants used for individual species and lumped components have been discussed above.

The effective SOA yield analysis did not account for differences in OA concentrations. However, The effect of OA concentrations on SOA yields are expected to be small given the relatively range of OA concentrations – e.g. the median OA concentration was 12, 6 and 4 μg/m^3 for experiments with pre-LEV, LEV and ULEV vehicles, respectively. For this concentration range, published yield curve indicate less than a factor of 2 variation in partitioning based on typical aromatic yield curves of aromatics (20, 33). This is much too small to explain the trends in effective yield with vehicle class. In addition, any shifts in partitioning (pre-LEV has highest OA concentration and therefore partitioning shifted the most to particle phase) are in the opposite direction to the actual yields. In other words, we measure the highest yield (ULEV vehicles) in the experiments with the lowest OA concentrations. Therefore the trends in Fig 1C are not due to a partitioning bias. If anything partitioning effects may (modestly) offsetting some of the trend.

Ambient Organic Carbon (OC) in Los Angeles. The ambient OC concentrations in Los Angeles were measured at the PM2.5 Chemical Speciation Network monitoring site (1630 N MAIN ST, LOS ANGELES, CA). These data were downloaded from the EPA Air Quality System data website (http://aqsdr1.epa.gov/aqsweb/aqstmp/airdata/download_files.html). OC was

collected by a quartz filter using a Met One SSAS sampler and analyzed using the NIOSH method from 2003 to 2006. From 2007 to 2016, OC was collected by a quartz filter using a URG 3000 sampler and analyzed using the IMPROVE method. OC measured by the NIOSH method was reconciled with the IMPROVE method by classifying OC in OC4 as black carbon based on the results from Chow et al.(36). OC was converted to OA assuming an organic mass to organic carbon ratio of 1.7(37).

References:

1. Gordon TD, *et al.* (2014) Secondary organic aerosol formation exceeds primary particulate matter emissions for light-duty gasoline vehicles. *Atmos. Chem. Phys.* 14(9):4661-4678.
2. May AA, *et al.* (2014) Gas- and particle-phase primary emissions from in-use, on-road gasoline and diesel vehicles. *Atmos. Environ.* 88:247-260.
3. Scanlon JT & Willis JT (1985) Calculation of Flame Ionization Detector Relative Response Factors Using the Effective Carbon Number Concept. *J. Chromatogr. Sci.* 23(333-340).
4. Maddox C (2007) *Carlifornia Air Resources Board Procedure for the Determination of C2 to C12 Hydrocarbons in Automotive Exhaust Samples by Gas Chromatography. Standard Operating Procedure No. MLD 102/103 Version 2.2.* http://www.arb.ca.gov/testmeth/slb/sop102-103v2-2.pdf.
5. CARB (2005) *California Air Resources Board Procedure for the Analysis of Automotive Exhaust for Methanol and Ethanol. MLD 101.* http://www.arb.ca.gov/testmeth/slb/exhaust.htm.
6. CARB (2006) *California Air Resouces Board Determination of Aldehyde and Ketone Compounds in Automotive Source Samples by High Performance Liquid Chromatography MLD104.* http://www.arb.ca.gov/testmeth/slb/exhaust.htm.
7. Zhao Y, *et al.* (2014) Intermediate-Volatility Organic Compounds: A Large Source of Secondary Organic Aerosol. *Environ. Sci. Technol.* 48(23):13743-13750.
8. Zhao Y, *et al.* (2016) Intermediate Volatility Organic Compound Emissions from On-Road Gasoline Vehicles and Small Off-Road Gasoline Engines. *Environ. Sci. Technol.* 50:4554-4563.
9. Kleno JG, Wolkoff P, Clausen PA, Wilkins CK, & Pedersen T (2002) Degradation of the adsorbent Tenax TA by nitrogen oxides, ozone, hydrogen peroxide, OH radical, and limonene oxidation products. *Environ. Sci. Technol.* 36(19):4121-4126.
10. Worton DR, *et al.* (2014) Lubricating Oil Dominates Primary Organic Aerosol Emissions from Motor Vehicles. *Environ. Sci. Technol.* 48(7):3698-3706.
11. CARB (2012) *California Air Resources Board, "LEV III" Amendments to the California Greenhouse Gas and Criteria Pollution Exhaust and Evaporative Emission Standards and Test Procedures and to the On-Board Diagnostic System Requirements for Passenger Cars, Light-Duty Trucks, and Medium-Duty Vehicles, and to the Evaporative Emission Requirements for Heavy-Duty Vehicles.* http://www.arb.ca.gov/regact/2012/leviiighg2012/levfrorev.pdf.
12. Hennigan CJ, *et al.* (2011) Chemical and physical transformations of organic aerosol from the photo-oxidation of open biomass burning emissions in an environmental chamber. *Atmos. Chem. Phys.* 11(15):7669-7686.
13. Dunlea EJ, *et al.* (2007) Evaluation of nitrogen dioxide chemiluminescence monitors in a polluted urban environment. *Atmos. Chem. Phys.* 7(10):2691-2704.

14. Hildebrandt L, Donahue NM, & Pandis SN (2009) High formation of secondary organic aerosol from the photo-oxidation of toluene. *Atmos. Chem. Phys.* 9(9):2973-2986.
15. Tkacik DS*, et al.* (2014) Secondary Organic Aerosol Formation from in-Use Motor Vehicle Emissions Using a Potential Aerosol Mass Reactor. *Environ. Sci. Technol.* 48(19):11235-11242.
16. Zhang X*, et al.* (2014) Influence of vapor wall loss in laboratory chambers on yields of secondary organic aerosol. *Proc. Natl. Acad. Sci. U. S. A.* 111:5802-5807.
17. Saleh R, Donahue NM, & Robinson AL (2013) Time Scales for Gas-Particle Partitioning Equilibration of Secondary Organic Aerosol Formed from Alpha-Pinene Ozonolysis. *Environ. Sci. Technol.* 47(11):5588-5594.
18. Trump ER, Riipinen I, & Donahue NM (2014) Interactions between atmospheric ultrafine particles and secondary organic aerosol mass: a model study. *Boreal Environment Research* 19(5-6):352-362.
19. Krechmer JE, Pagonis D, Ziemann PJ, & Jimenez JL (2016) Quantification of Gas-Wall Partitioning in Teflon Environmental Chambers Using Rapid Bursts of Low-Volatility Oxidized Species Generated in Situ. *Environ. Sci. Technol.* 50(11):5757-5765.
20. Chan AWH*, et al.* (2009) Secondary organic aerosol formation from photooxidation of naphthalene and alkylnaphthalenes: implications for oxidation of intermediate volatility organic compounds (IVOCs). *Atmos. Chem. Phys.* 9(9):3049-3060.
21. Carter WPL (2010) Development of the SAPRC-07 chemical mechanism. *Atmos. Environ.* 44(40):5324-5335.
22. Carlton AG*, et al.* (2010) Model Representation of Secondary Organic Aerosol in CMAQv4.7. *Environ. Sci. Technol.* 44(22):8553-8560.
23. Keywood MD, Varutbangkul V, Bahreini R, Flagan RC, & Seinfeld JH (2004) Secondary organic aerosol formation from the ozonolysis of cycloalkenes and related compounds. *Environ. Sci. Technol.* 38(15):4157-4164.
24. Gong HM, Matsunaga A, & Ziemann PJ (2005) Products and mechanism of secondary organic aerosol formation from reactions of linear alkenes with NO3 radicals. *J. Phys. Chem. A* 109(19):4312-4324.
25. Song C, Na K, Warren B, Malloy Q, & Cocker DR (2007) Impact of propene on secondary organic aerosol formation from m-xylene. *Environ. Sci. Technol.* 41(20):6990-6995.
26. Atkinson R & Arey J (2003) Atmospheric degradation of volatile organic compounds. *Chem. Rev. (Washington, DC, U. S.)* 103(12):4605-4638.
27. Kwok ESC & Atkinson R (1995) Estimation of Hydroxyl Radical Reaction-Rate Constants for Gas-Phase Organic-Compounds Using a Structure-Reactivity Relationship - an Update. *Atmos. Environ.* 29(14):1685-1695.
28. Hunter JF, Carrasquillo AJ, Daumit KE, & Kroll JH (2014) Secondary Organic Aerosol Formation from Acyclic, Monocyclic, and Polycyclic Alkanes. *Environmental Sciene and Technology* 48:10227-10234.

29. Lim YB & Ziemann PJ (2009) Effects of Molecular Structure on Aerosol Yields from OH Radical-Initiated Reactions of Linear, Branched, and Cyclic Alkanes in the Presence of NOx. *Environ. Sci. Technol.* 43(7):2328-2334.
30. Presto AA, Miracolo MA, Donahue NM, & Robinson AL (2010) Secondary Organic Aerosol Formation from High-NOx Photo-Oxidation of Low Volatility Precursors: n-Alkanes. *Environ. Sci. Technol.* 44(6):2029-2034.
31. Cappa CD*, et al.* (2013) Application of the Statistical Oxidation Model (SOM) to Secondary Organic Aerosol formation from photooxidation of C-12 alkanes. *Atmos. Chem. Phys.* 13(3):1591-1606.
32. Zhao Y*, et al.* (2015) Intermediate Volatility Organic Compound Emissions from On-Road Diesel Vehicles: Chemical Composition, Emission Factors, and Estimated Secondary Organic Aerosol Production. *Environ. Sci. Technol.* 49(19):11516-11526.
33. Ng NL*, et al.* (2007) Secondary organic aerosol formation from m-xylene, toluene, and benzene. *Atmos. Chem. Phys.* 7(14):3909-3922.
34. Loza CL*, et al.* (2014) Secondary organic aerosol yields of 12-carbon alkanes. *Atmos. Chem. Phys.* 14(3):1423-1439.
35. Gentner DR*, et al.* (2012) Elucidating secondary organic aerosol from diesel and gasoline vehicles through detailed characterization of organic carbon emissions. *Proc. Natl. Acad. Sci. U. S. A.* 109(45):18318-18323.
36. Chow JC*, et al.* (2007) The IMPROVE-A temperature protocol for thermal/optical carbon analysis: maintaining consistency with a long-term database. *J. Air Waste Manage. Assoc.* 57(9):1014-1023.
37. McDonald BC, Goldstein AH, & Harley RA (2015) Long-Term Trends in California Mobile Source Emissions and Ambient Concentrations of Black Carbon and Organic Aerosol. *Environ. Sci. Technol.* 49(8):5178-5188.
38. Carlton AG, Pinder RW, Bhave PV, & Pouliot GA (2010) To What Extent Can Biogenic SOA be Controlled? *Environ. Sci. Technol.* 44(9):3376-3380.
39. Carter WPL (2012) SAPRC-07 and SAPRC-11 Chemical Mechanisms, Test Simulations, and Environmental Chamber Simulation Files:SAPRC07.XLS. http://www.engr.ucr.edu/~carter/SAPRC/SAPRCfiles.htm.
40. USEPA (2014) Estimation Programs Interface Suite
41. Reisen F & Arey J (2002) Reactions of hydroxyl radicals and ozone with acenaphthene and acenaphthylene. *Environ. Sci. Technol.* 36(20):4302-4311.
42. Kwok ESC, Atkinson R, & Arey J (1997) Kinetics of the gas-phase reactions of indan, indene, fluorene, and 9,10-dihydroanthracene with OH radicals, NO3 radicals, and O-3 (vol 29, pg 299, 1997). *Int. J. Chem. Kinet.* 29(8):645-645.
43. Lee W, Stevens PS, & Hites RA (2003) Rate constants for the gas-phase reactions of methylphenanthrenes with OH as a function of temperature. *J. Phys. Chem. A* 107(34):6603-6608.
44. Ananthula R, Yamada T, & Taylor PH (2006) Kinetics of OH radical reaction with anthracene and anthracene-d(10). *J. Phys. Chem. A* 110(10):3559-3566.
45. Kameda T*, et al.* (2013) Prediction of rate constants for the gas phase reactions of triphenylene with OH and NO3 radicals using a relative rate method in CCl4 liquid phase-system. *Chemosphere* 90(2):766-771.

Supplemental Figures:

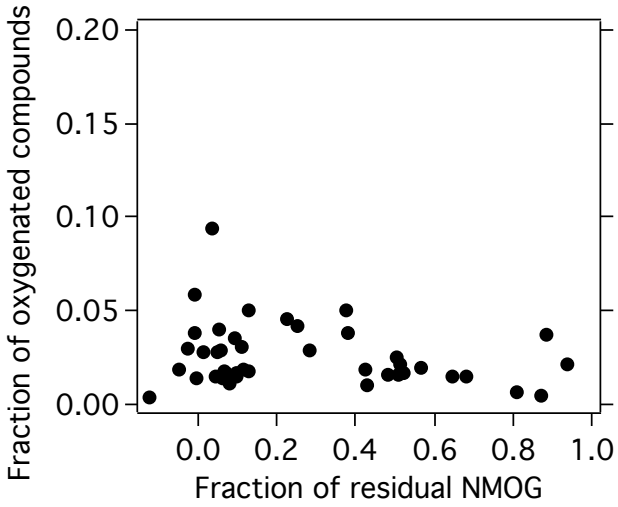

Figure S1. Mass fraction of total oxygenated compounds in NMOG as a function of the fraction of the residual NMOG. Data are only shown for tests in which all measurements of VOCs, IVOCs, SVOCs and oxygenated compounds were carried out.

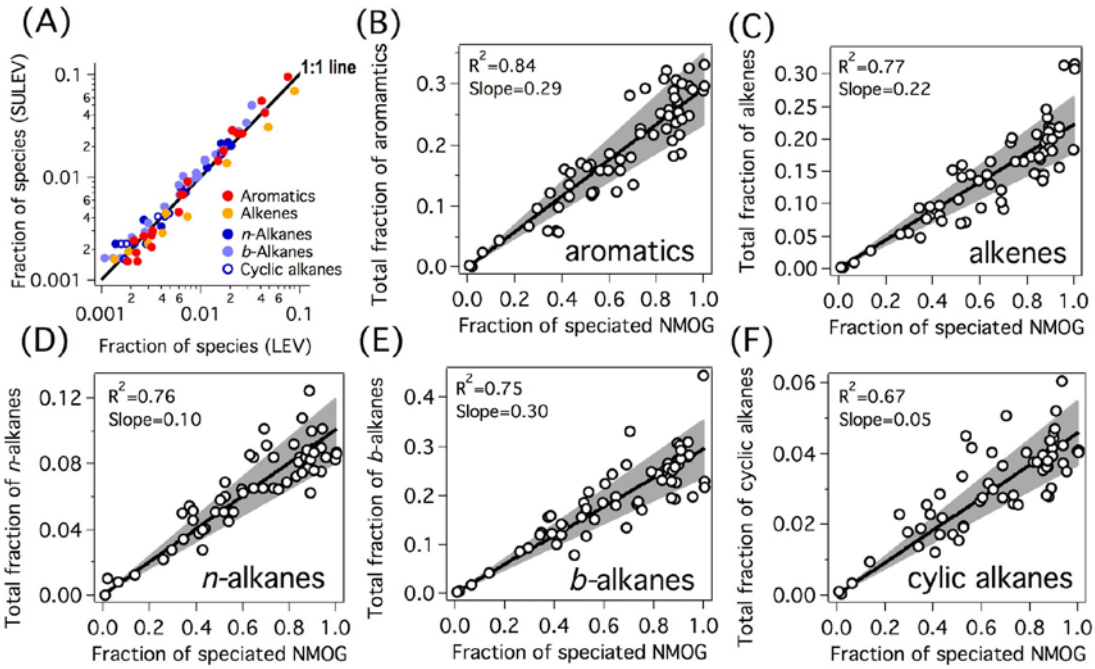

Figure S2. (A) Comparison of speciated VOC emissions from a SULEV and LEV vehicle. The fraction of speciated VOCs in total NMOG is 35% for the SULEV vehicle and 91% for the LEV vehicle. This comparison includes 66 individual species, including 20 aromatic compounds, 12 alkenes, 9 *n*-alkanes, 28 *b*-alkanes and 11 cyclic alkanes. The figure shows the consistency in the composition of the organic emissions between vehicles in spite of the fractions of speciated VOCs. (B)-(F) Correlation of total speciated VOCs with the sum of species in each major component across all tests with speciation analysis of NMOG: (B) single-ring aromatics (SRA), (C) alkenes, (D) *n*-alkanes, (E) *b*-alkanes and (F) cyclic alkanes. All data are presented as a mass fraction of total NMOGs. Each symbol represents one test. The grey-shaded area in (B)-(F) indicates ±20% range of the slope. The strong correlations showed in (B)-(F) support the conclusion that the chemical composition of speciated VOCs is consistent between different vehicles.

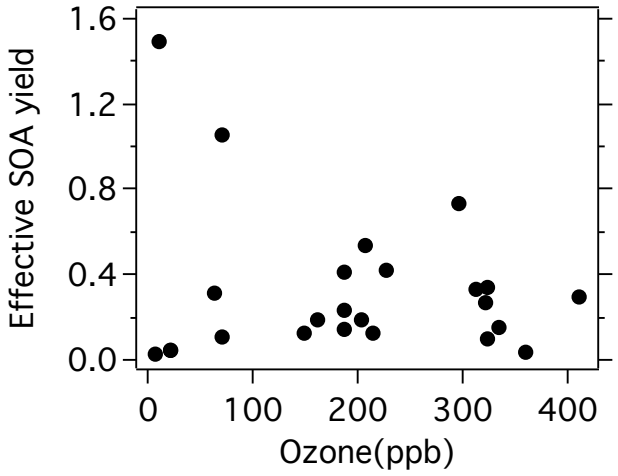

Figure S3. Scatter plot of effective SOA yields versus ozone concentrations at the end of experiments. There is no relationship indicating that unsaturated compounds are not an important class of SOA precursors in these experiments.

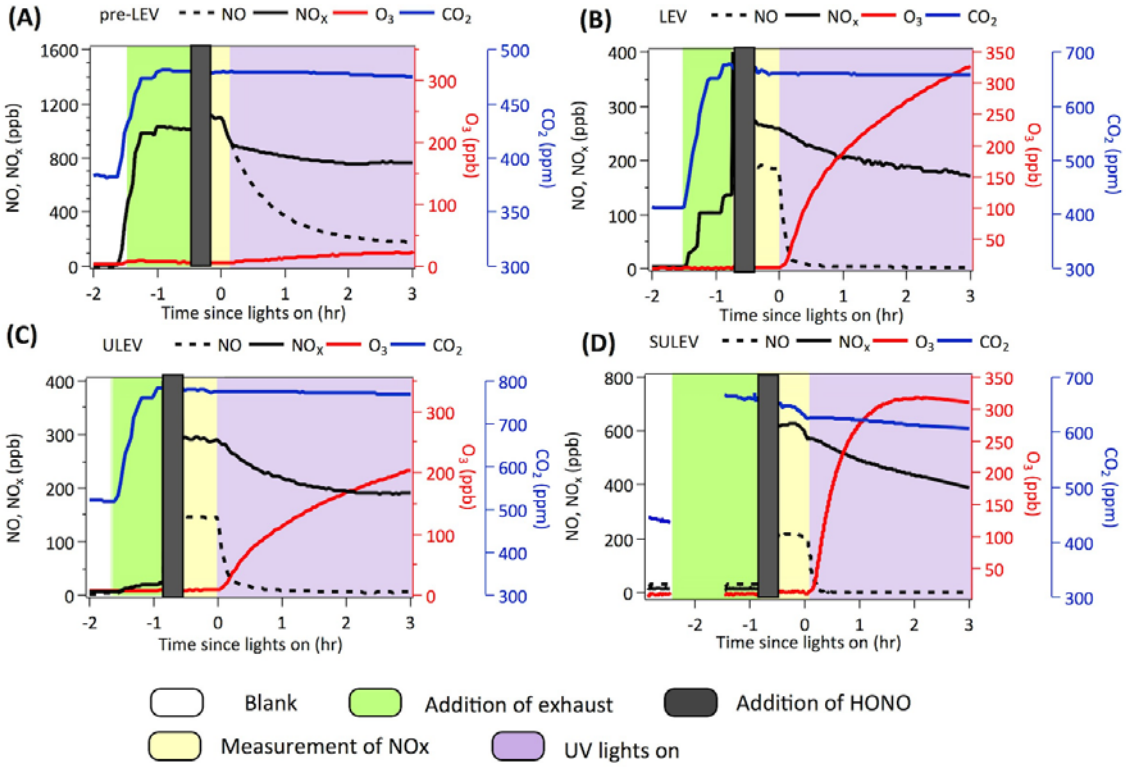

Figure S4. Time series of measured gas concentrations during chamber experiments. Gas concentrations were not monitored during the addition of exhaust phase of the experiments with SULEV vehicles because the gas monitors were sampling from a potential aerosol mass reactor. For the SULEV experiments, gas concentrations in the chamber were measured before the UV lights were turned on to initiate the photo-oxidation. NO_x measurements were made with a chemiluminescence NOx analyzer. The NO_x data includes interferences from HONO added to chamber, as discussed in the main text.

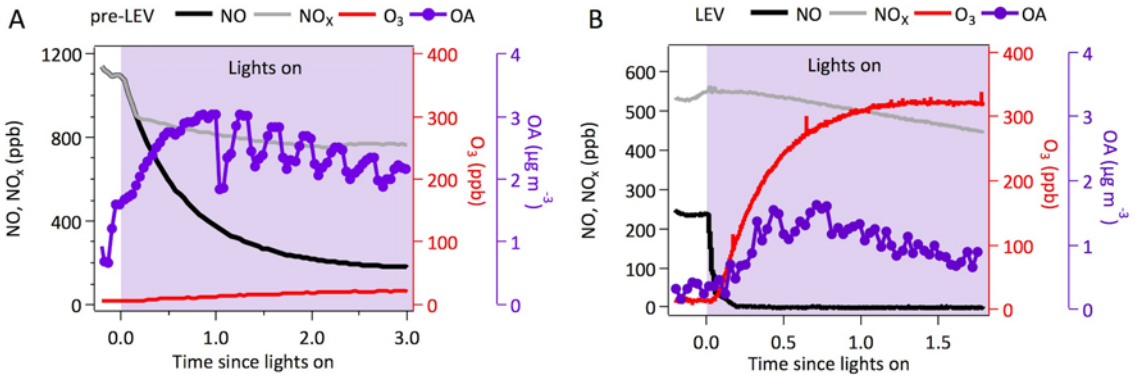

Figure S5. Measured evolution of gases and OA during the photo-oxidation phase of smog chamber experiments with a pre-LEV and LEV vehicle. (These data are no wall loss corrected). The repeated dips in OA in (A) were due to alternate sampling between a bypass and a thermal denuder line. Substantial SOA was produced during experiments with pre-LEV vehicles with high NO concentrations inside the chamber. NO_x measurements were made with a chemiluminescence NOx analyzer. The NO_x data includes interferences from HONO added to chamber, as discussed in the main text.

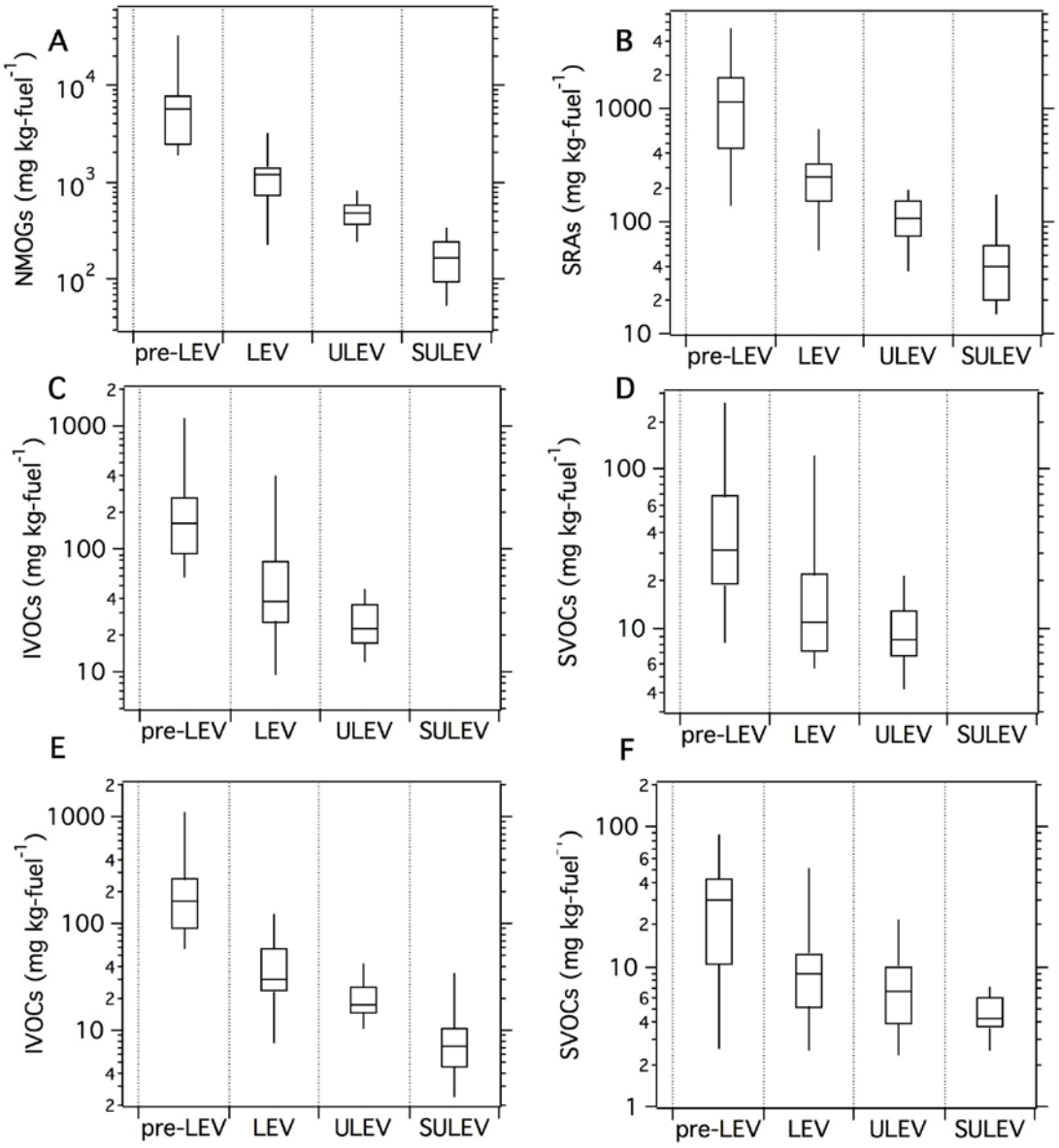

Figure S6. NMOG and SOA precursor emission factors for all tested vehicles. The boxes represent the 75th and 25th percentiles with the centerline being the median. The whiskers are the 90th and 10th percentiles. The data used to generate this figure are listed in Datasets S1-S3. (A)~(D) present measured data. (E) and (F) present a combination of measured and estimated data of IVOCs and SVOCs.

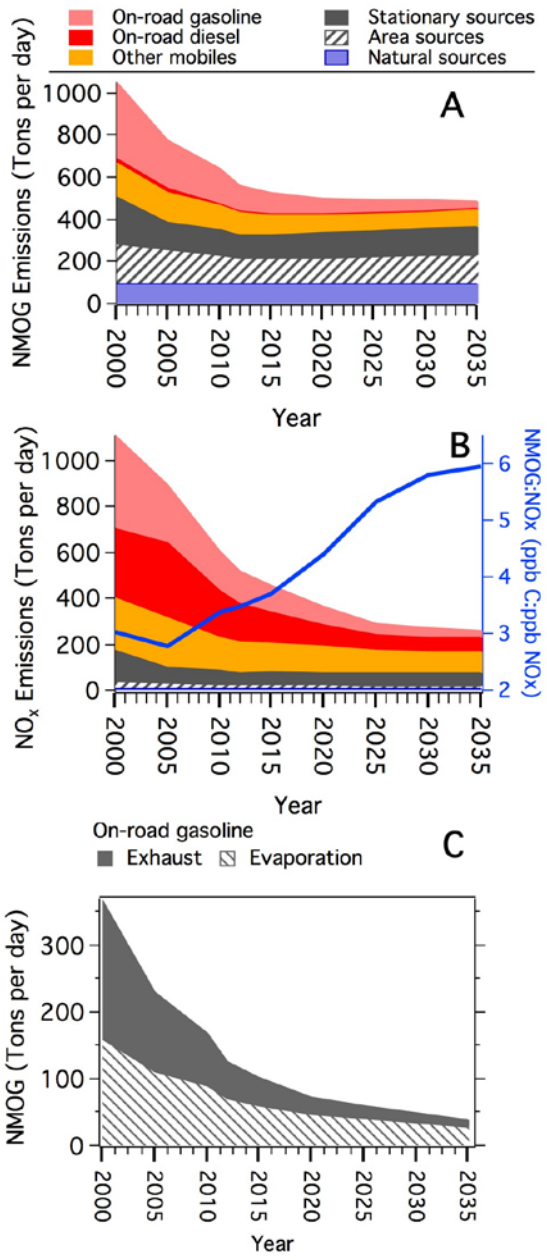

Figure S7. Emissions of (A) NMOG and (B) NO_x from sources in the South Coast Air Basin, California with the base year of 2012. (CARB Emission Inventory data; http://www.arb.ca.gov/app/emsinv/fcemssumcat2013.php). Panel (B) also presents the NMOG:NO_x calculated based on projected NMOG and NO_x emissions. Panel (C) shows the split of gasoline vehicle NMOG emissions into evaporation and exhaust. The split is based on the CARB EMFAC2014 model (http://www.arb.ca.gov/emfac/2014/).

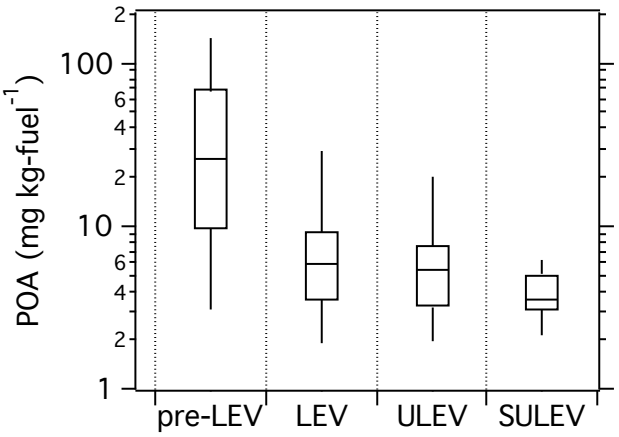

Figure S8. POA emission factors for all tested vehicles. POA is defined as the organics collected by a bare quartz filter assuming an organic mass to organic carbon ratio of 1.2.

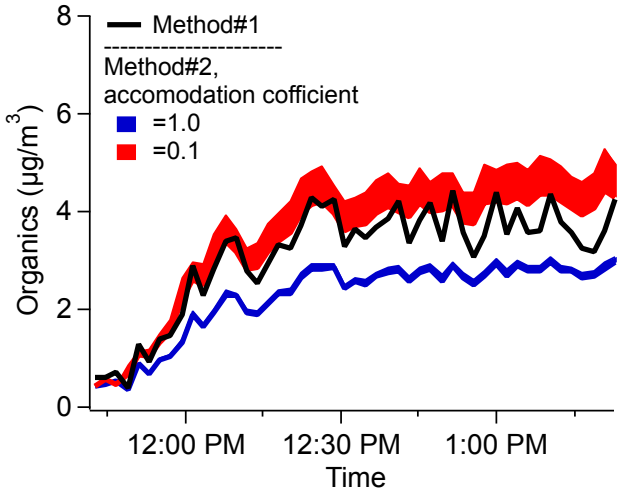

Figure S9. SOA production calculated using different approaches to correct for vapor wall losses in a photo-oxidation experiment for a ULEV vehicle. Method#1 assumes that condensable vapors maintain equilibrium with both suspended and wall-bound particles. Method#2 estimates the vapor wall losses based on the condensation sink of suspended particles and chamber walls. The mass accommodation coefficients of 0.1 and 1 are used for suspended particles in Method#2. The shaded areas indicate the estimated SOA production range when the condensation sink of the chamber walls is between 0.10 and 0.14 min^{-1} for each mass accommodation coefficient. These comparisons show that our approach of determining SOA production (method#1) accounts for vapor wall losses if the published condensational sink of the chamber walls (19) is applicable to our chamber.

Supplemental Tables:

Table S1. Summary of the test fleet and measurements.

Test ID[1]	*Vehicle name*	*Vehicle class*[2]	*Model year*	*Engine size (L)*	*Certification*	*Measured fuel economy (MPG)*	*Test cycle*	*Notes*[3]
1027837	PreLEV-1	PC	1996	2.7	Tier I	20.01	Cold UC	a,b,c
1027852	ULEV-13	LDT	2010	3.6	ULEV; Tier II	15.61	Cold UC	a,b,c
1027859	PreLEV-1	PC	1996	2.7	Tier I	20.39	Cold UC	a,b
1027863	ULEV-3	PC	2008	1.6	LEV2, ULEV; Tier II, Bin 5	25.54	Cold UC	a,b,c
1027872	PreLEV-7	PC	1993	4.9	Tier I	13.09	Cold UC	a,b,c
1027905	ULEV-6	PC	2009	2	LEV2, ULEV; Tier II, Bin 5	19.75	Cold UC	a,b,c
1027906	LEV-13	PC	2008	3.6	LEV2; Tier II, Bin 5	18.59	Cold UC	a,b
1027907	ULEV-8	PC	2009	2.4	LEV2, ULEV	18.75	Cold UC	a,b,c
1027908	LEV-17	PC	2004	2.2	LEV2; Tier II, Bin 8	24.68	Cold UC	b,c
1027918	LEV-10	PC	2003	3.5	LEV1, NLEV	18.31	Cold UC	a,b,c
1027920	PreLEV-13	PC	1991	3.8	Tier I	18.46	Cold UC	a,b,c
1027921	PreLEV-6	PC	1992	3.8	Tier I	17.97	Cold UC	a,b,c
1027969	LEV-3	PC	2000	3.5	LEV1	18.81	Cold UC	b,c
1027970	ULEV-1	PC	2003	1.8	LEV1, ULEV	26.78	Cold UC	a,b,c
1027971	ULEV-13	LDT	2010	3.6	ULEV; Tier II	15.78	Cold UC	a,b,c,d
1027973	ULEV-2	PC	2005	1.8	LEV2, ULEV; Tier II, Bin 5	26.23	Cold UC	a,b,c
1027975	LEV-2	LDT	1999	4	LEV1, NLEV	16.39	Cold UC	a,b
1027976	PreLEV-3	PC	1994	1.9	LEV1; Tier I	21.67	Cold UC	b,c
1027977	ULEV-4	PC	2008	2.7	LEV2	17.78	Cold UC	b,c
1027978	LEV-12	LDT	2005	2.7	LEV2; Tier II, Bin 5	19.31	Cold UC	b

Test ID[1]	*Vehicle name*	*Vehicle class*[2]	*Model year*	*Engine size (L)*	*Certification*	*Measured fuel economy (MPG)*	*Test cycle*	*Notes*[3]
1028021	ULEV-5	LDT	2009	5.7	Tier II	13.78	Cold UC	a,b,c
1028022	ULEV-7	LDT	2008	4.2	LEV2	15.44	Cold UC	a,b,d
1028023	PreLEV-2	PC	2003	3	LEV1; Tier I	17.31	Cold UC	a,b,c
1028027	LEV-1	PC	1998	1.8	LEV1, TLEV	27.31	Cold UC	a,b
1028029	PreLEV-5	PC	1992	3.4	Tier I	15.70	Cold UC	a,b
1028075	LEV-3	PC	2000	3.5	LEV1	20.12	Cold UC	a,b,c
1032282	ULEV-16	PC	2011	3.6	LEV2, ULEV	15.76	Cold UC	a,b
1032283	ULEV-11	PC	2008	3.5	LEV2	15.24	Cold UC	a,b,d
1032302	LEV-4	PC	1997	3	LEV	19.34	Cold UC	a,b,c
1032303	PreLEV-10	PC	1990	5	Tier I	13.06	Cold UC	b,c,d
1032304	LEV-4	PC	1997	3	LEV	19.21	Cold UC	a,b,c,d
1032309	ULEV-16	PC	2011	3.6	LEV2, ULEV	15.76	Cold UC	a,b,c,d
1032310	ULEV-9	PC	2011	n/a	LEV2, ULEV	20.38	Cold UC	a,b
1032320	LEV-18	PC	1991	3.8	LEV	19.36	Cold UC	a,b,c
1032321	ULEV-16	PC	2011	3.6	LEV2, ULEV	15.76	Cold UC	a,b,c,d
1032342	ULEV-14	PC	2011	2	ULEV	21.09	Cold UC	a,b,c,d
1032346	LEV-7	PC	1998	3	LEV	18.78	Cold UC	a,b,d
1032351	ULEV-14	PC	2011	2	ULEV	22.30	Cold UC	a,b,d
1032360	ULEV-11	PC	2008	3.5	LEV2	20.44	Hot UC	a,b,c,d
1032383	ULEV-10	PC	2012	3.6	ULEV	19.62	Cold UC	a,b,c
1032388	LEV-5	PC	2001	2.2	LEV	21.81	Cold UC	a,b,c
1032392	PreLEV-11	PC	1989	1.3	Tier I	27.21	Cold UC	a,b,c
1032393	LEV-9	PC	1999	2	TLEV	23.57	Cold UC	a,b,c,d
1032394	LEV-6	PC	2002	5.7	LEV	N/A	Cold UC	b,c

Test ID[1]	*Vehicle name*	*Vehicle class*[2]	*Model year*	*Engine size (L)*	*Certification*	*Measured fuel economy (MPG)*	*Test cycle*	*Notes*[3]
1032428	LEV-11	N/A	N/A	N/A	N/A	N/A	Cold UC	b,c
1032440	PreLEV-9	PC	1988	1.6	Tier I	24.12	Cold UC	b,c,d
1032442	PreLEV-4	PC	1987	4.1	Tier I	14.58	Cold UC	a,b,c
1032443	PreLEV-14	PC	1991	4	Tier I	16.45	Cold UC	a,b,c
1032444	PreLEV-9	PC	1988	1.6	Tier I	23.78	Cold UC	a,b,c
1032445	PreLEV-8	LDT	1993	4.3	Tier I	14.98	Cold UC	a,b,c
1032472	LEV-6	PC	2002	5.7	LEV	9.72	Cold UC	a,b,c
1032473	LEV-4	PC	1997	3	LEV	19.05	Hot UC	a,b,d
1038708	SULEV-3	PC (GDI)	2012	2	SULEV	23.76	Cold UC	a
1038723	SULEV-8	PC (GDI)	2014	3.5	LEV2, SULEV	19.84	Cold UC	a,d
1038724	SULEV-9	PC (GDI)	2012	2.4	SULEV	21.08	Cold UC	d
1038747	SULEV-4	PC (GDI)	2013	1.4	PZEV	36.72	Cold UC	a,d
1038755	SULEV-5	PC	2012	2.5	PZEV	35.17	Cold UC	a,d
1038801	ULEV-17	PC (GDI)	2013	1.6	ULEV	27.50	Cold UC	a,d
1038821	LEV-14	PC	2008	3.9	LEV2 LEV	15.80	Cold UC	a
1038822	ULEV-18	PC (GDI)	2013	1.6	LEV2, ULEV	23.66	Cold UC	a,d
1038824	ULEV-12	LDT	2013	5.3	ULEV	12.78	Cold UC	a
1038825	LEV-16	PC (GDI)	2012	1.6	LEV2, LEV	24.48	Cold UC	a,d
1038827	ULEV-15	PC (GDI)	2013	2	LEV2, ULEV	26.32	Cold UC	a
1038848	LEV-14	PC	2008	3.9	LEV2, LEV	15.76	Cold UC	d
1038849	LEV-14	PC	2008	3.9	LEV2, LEV	15.64	Cold UC	a
1038853	SULEV-1	PC (GDI)	2014	2.4	PZEV	6.92	Cold UC	d
1038862	SULEV-6	PC (GDI)	2013	3.6	LEV2, SUL	16.86	Cold UC	a,d
1038867	SULEV-7	PC (GDI)	2012	2.4	PZEV	21.55	Cold UC	a,d

Test ID[1]	*Vehicle name*	*Vehicle class*[2]	*Model year*	*Engine size (L)*	*Certification*	*Measured fuel economy (MPG)*	*Test cycle*	*Notes*[3]
1038891	LEV-8	M3	2003	5.4	LEV	11.43	Cold UC	a,d
1038901	PreLEV-12	PC	1990	3.8	TIER0	17.65	Cold UC	a,d
1038909	ULEV-19	PC (GDI)	2013	2	ULEV	19.42	Cold UC	a
1038917	ULEV-12	LDT	2013	5.3	ULEV	12.93	Cold UC	a
1038918	ULEV-12	LDT	2013	5.3	ULEV	12.73	Cold UC	d
1038920	SULEV-1	PC (GDI)	2014	2.4	PZEV	23.39	Cold UC	a,d
1038945	ULEV-12	LDT	2013	5.3	ULEV	12.60	Cold UC	a
1038947	ULEV-18	PC (GDI)	2013	1.6	LEV2, ULEV	23.81	Cold UC	a,d
1038952	SULEV-6	PC (GDI)	2013	3.6	LEV2, SULEV	17.52	Cold UC	a,d
1038980	LEV-15	PC	2007	1.8	LEV2, LEV	25.18	Cold UC	a

[1] Complete data for tests with IDs ranging 1027837 to 1032473 are reported in May et al. (2), Zhao et al. (3), and Gordon et al. (1). The tests with test IDs ranging from 1038708 to 1038980 were newly conducted with a focus on newer vehicles (ULEV and SULEV).
[2] PC: passenger car; LDT: light-duty truck; GDI: gasoline direct injection
[3] Note: Different measurements have been carried out for each test: "a" refers to speciated analysis of NMOGs; "b" and "c" refer to quantification of IVOCs and SVOCs; and "d" refers to photo-oxidation experiment.

Table S2. Conditions inside the smog chamber during photo-oxidation experiments.

Test ID	*Vehicle*	*NMOG (ppb)*	*Propene (ppm)*	*d-butanol (ppm)*	*NO (ppb)*	*OH exposure (molecules cm^{-3} hr)*	*OA ($\mu g\ m^{-3}$)*
1038901	PreLEV-12	969	0.60	0.06	546	1.69E+07	4.7
1032442	PreLEV-4	1401	0.13	0.06	671	6.77E+06	5.1
1032440	PreLEV-9	10641	0.00	0.06	2503	5.54E+06	19.8
1032444	PreLEV-9	4358	0.00	0.06	1099	6.75E+06	12.3
1032303	PreLEV-10	2479	1.00	0.06	1503	7.68E+06	37.8
1038848	LEV-14	617	0.73	0.06	236	4.50E+06	2.5
1038825	LEV-16	134	0.93	0.06	196	1.87E+07	3.1
1038891	LEV-8	366	0.53	0.06	295	1.74E+07	15.2
1032304	LEV-4	316	0.20	0.12	207	8.87E+06	7.0
1032473	LEV-4	83	0.27	0.06	185	7.55E+06	2.6
1032346	LEV-7	685	0.73	0.06	687	8.07E+06	10.4
1032393	LEV-9	192	0.53	0.06	401	7.97E+06	6.1
1038801	ULEV-17	203	0.53	0.06	119	1.04E+07	2.9
1038822	ULEV-18	237	0.53	0.06	107	7.47E+06	1.8
1038918	ULEV-12	299	0.47	0.06	237	6.40E+06	3.1
1028022	ULEV-7	260	0.25	0.00	83	1.18E+07	13.3
1032283	ULEV-11	100	0.51	0.06	146	1.02E+07	7.1
1032360	ULEV-11	59	0.20	0.06	146	8.30E+06	1.2
1032359	ULEV-11	76	0.27	0.06	137	1.05E+07	3.4
1027971	ULEV-13	140	0.06	0.06	41	1.05E+07	15.5
1032342	ULEV-14	143	0.60	0.06	303	1.03E+07	8.6
1032351	ULEV-14	276	0.47	0.06	305	1.38E+07	4.5

Test ID	*Vehicle*	*NMOG (ppb)*	*Propene (ppm)*	*d-butanol (ppm)*	*NO (ppb)*	*OH exposure (molecules cm^{-3} hr)*	*OA ($\mu g\ m^{-3}$)*
1032309	ULEV-16	196	0.13	0.06	97	1.17E+07	2.9
1032321	ULEV-16	287	0.13	0.06	122	1.76E+07	4.4
1038853	SULEV-1	55	0.33	0.06	137	1.98E+07	0.0
1038920	SULEV-1	68	0.60	0.06	258	1.07E+07	0.0
1038747	SULEV-4	31	0.53	0.06	108	5.46E+06	0.3
1038755	SULEV-5	50	0.53	0.06	168	1.04E+07	0.4
1038867	SULEV-7	77	0.53	0.06	149	6.67E+06	0.1
1038862	SULEV-6	57	0.40	0.06	194	1.25E+07	0.5
1038952	SULEV-6	51	0.43	0.06	193	4.90E+06	0.0
1038723	SULEV-8	81	N/A	0.06	N/A	4.51E+06	0.0
1038724	SULEV-9	52	1.24	0.06	59	6.41E+06	0.5

Note: 1) NO concentrations in all experiments, except for the one with Test ID of 1032440, were directly measured in the smog chamber. The NO concentration in the experiment with Test ID of 1032440 was calculated from the NO concentration in the CVS and the dilution ratio because NO concentration in the smog chamber was out of the measurement range.

Table S3. Parameters for VOC SOA yields under high-NO_x conditions from Carlton et al.(38).

	α_1	C_1*($\mu g/m^3$)	α_2	C_2*($\mu g/m^3$)
Alk5	0.0718	0.02		
Benzene	0.0942	0.302	1.162	111.11
ARO1	0.0758	2.326	0.1477	21.277
ARO2	0.0386	1.314	0.1119	34.483

Table S4. SOA yields under low-NO_x conditions (single-ring aromatics from Ng et al.(33) and naphthalenes from Chan et al.(20))

	SOA Yield
Benzene	0.37
ARO1	0.36
ARO2	0.3
Naphthalene	0.73
1-methylnaphthalene	0.68
2-methylnaphthalene	0.58

Table S5. OH reaction rate constants of SOA precursors in VOCs from SAPRC-07(39).

	OH rate constant (cm^3 $molec^{-1}$ s^{-1})
ALK5	9.40E-12
Benzene	1.22E-12
ARO1	6.15E-12
ARO2	2.57E-11

Table S6. Parameters for n-alkane SOA yields under high-NO_x conditions derived from results of Presto et al. **(30)**.

	C10	C11	C12	C13	C14	C15	C16	C17	C18	C19	C20	C21	C22	C23
α	C* (μg/m^3)													
0.063	32.26	10.20	3.23	0.49	0.25	0.17	0.13	0.10	0.09	0.08	0.07	0.06	0.05	0.05
0.089	322.58	102.01	32.26	4.87	2.50	1.70	1.29	1.00	0.88	0.76	0.68	0.59	0.54	0.49
0.55	3225.81	1020.09	322.58	48.69	25.03	16.95	12.86	10.00	8.80	7.65	6.77	5.95	5.36	4.88
0.2	32258.10	10200.90	3225.81	486.90	250.30	169.50	128.57	100.00	87.98	76.49	67.74	59.47	53.61	48.80

Table S7. Parameters for SOA yields of naphthalenes under high-NO_x conditions from Chan et al.(20).

	α_1	C_1*(μg/m^3)	α_2	C_2*(μg/m^3)
Naphthalene	0.21	1.69	1.07	270.27
1-methylnaphthalene	0.5	9.09		
2-methylnaphthalene	0.55	7.69		
1,2-dimethylnaphthalene	0.31			

Table S8. Surrogate compounds for predicting SOA production from unspeciated IVOCs.

Table S8a. Surrogate compounds (*n*-alkanes) used for OH reaction rate constants (cm^3 $molec^{-1}$ s^{-1}) and SOA yields of unspeciated IVOC bins for the IVOC-cyclic case.

Bin#	OH rate constant	Surrogate compounds for SOA yields	
		Unspeciated *b*-alkanes	Unspeciated cyclic compounds (IVOC-cyclic)
B12	C12	C10	C12
B13	C13	C11	C13
B14	C14	C12	C14
B15	C15	C13	C15
B16	C16	C14	C16
B17	C17	C15	C17
B18	C18	C16	C18
B19	C19	C17	C19
B20	C20	C18	C20
B21	C21	C19	C21
B22	C22	C20	C22

Table S8b. Surrogate compounds (*n*-alkanes and naphthalenes) for OH reaction rate constants (cm^3 $molec^{-1}$ s^{-1}) and SOA yields of unspeciated cyclic compounds in each IVOC bin for the IVOC-aromatic case.

Bin#	OH rate constant	Unspeciated cyclic compounds (IVOC-aromatic)
B12	Naphthalene	Naphthalene
B13	C1-naphthalene	2-Methylnaphthalene
B14	C2-naphthalene	1,2-Dimethylnaphthalene
B15	C3-naphthalene	C15
B16	C4-naphthalene	C16
B17	C17	C17
B18	C18	C18
B19	C19	C19
B20	C20	C20
B21	C21	C21
B22	C22	C22

Table S9. OH reaction rate constants of speciated IVOCs (Estimation of SOA yield of each compound is described in Note#2).

Compound code	Compound name	OH reaction rate (cm^3 $molec^{-1}$ s^{-1})
1	Dodecane	1.32E-11
2	Tridecane	1.51E-11
3	Tetradecane	1.68E-11
4	Pentadecane	1.82E-11
5	Hexadecaen	1.96E-11
6	Heptadecane	2.10E-11
7	Octadecane	2.24E-11
8	Nonadecane	2.38E-11
9	Eicosane	2.52E-11
10	Heneicosane	2.67E-11
11	Docosane	2.81E-11
12	2,6,10-Trimethylundecane	1.70E-11
13	2,6,10-Trimethyldodecane	1.87E-11
14	2,6,10-Trimethyltridecane	2.01E-11
15	2,6,10-Trimethylpentadecane	2.30E-11
16	Pristane	2.44E-11
17	Phytane	2.61E-11
18	Hexylcylohexane	1.76E-11
19	Heptylcyclohexane	1.91E-11
20	Octylcyclohexane	2.05E-11
21	Nonylcyclohexane	2.19E-11
22	Decylcyclohexane	2.33E-11
23	Undecylcyclohexane	2.47E-11
24	Dodecylcyclohexane	2.61E-11
25	Tridecylcyclohexane	2.75E-11
26	Tetradecylcyclohexane	2.89E-11
27	Pentadecylcyclohexane	3.04E-11
28	Hexadecylcyclohexane	3.18E-11
29	Heptadecylcyclohexane	3.32E-11
30	Naphthalene	2.30E-11
31	2-methylnaphthalene	4.86E-11
32	1-methylnaphthalene	4.09E-11

Compound code	Compound name	OH reaction rate (cm^3 $molec^{-1}$ s^{-1})
33	C2-naphthalene	6.00E-11
34	C3-naphthalene	8.00E-11
35	C4-naphthalene	8.00E-11
36	Acenaphthylene	1.24E-10
37	Acenaphthene	8.00E-11
38	Fluorene	1.60E-11
39	C1-Fluorene	8.00E-11
40	Phenanthrene	3.20E-11
41	Anthracene	1.78E-10
42	C1-Phenanthrene/anthracene	5.89E-11
43	C2-Phenanthrene/anthracene	8.00E-11
44	Fluoranthene	3.30E-11
45	Pyrene	5.60E-11
46	C1-Fluoranthene/pyrene	1.31E-10
47	Pentylbenzene	1.01E-11
48	Hexylbenzene	1.15E-11
49	Heptylbenzene	1.30E-11
50	Octylbenzene	1.44E-11
51	Nonylbenzene	1.58E-11
52	Decylbenzene	1.72E-11
53	Undecylbenzene	1.86E-11
54	Dodecylbenzene	2.00E-11
55	Tridecylbenzene	2.14E-11
56	Tetradecylbenzene	2.29E-11
57	Pentadecylbenzene	2.43E-11

Note: 1) OH rate constant: Compound#1, 2, 30 from Atkinson and Arey(26); Compound#3~29 and 46~57 are calculated using the structure-reactivity relationship(27, 40); Compound#31~35, 39, 43 are from Chan et al.(20); Compound#36, 37 are from Reisen and Arey(41); Compound#38 is from Kwok et al.(42); Compound# 40 and 42 are from Lee et al.(43); Compound#41 is from Ananthula et al. (44)and Compound#43, 44 are from Kameda et al. (45)
2) SOA mass yields: Compound#1~11 are derived from results in Presto et al.(30); Compound#12-29 are derived based on the approach of Zhao et al.(7); Compound#30~46 is derived from the results in Chan et al. (20); Compound#47~57 are assumed to be the same as n-alkanes with the same carbon number.